

See discussions, stats, and author profiles for this publication at:  
<https://www.researchgate.net/publication/222993954>

# Reactivity, photochemistry and thermochemistry of simple metal—ligand ions in the gas phase

ARTICLE *in* POLYHEDRON · JANUARY 1988

Impact Factor: 2.01 · DOI: 10.1016/S0277-5387(00)81784-2

---

CITATIONS

87

---

READS

7

2 AUTHORS, INCLUDING:



Steven W Buckner

Saint Louis University

56 PUBLICATIONS 851 CITATIONS

SEE PROFILE

## REACTIVITY, PHOTOCHEMISTRY AND THERMOCHEMISTRY OF SIMPLE METAL-LIGAND IONS IN THE GAS PHASE

STEVEN W. BUCKNER and BEN S. FREISER†

Herbert C. Brown Laboratory of Chemistry, Purdue University, West Lafayette,  
IN 47907, U.S.A.

**Abstract**—In this review we discuss recent results from our laboratory on the chemistry, photochemistry and thermodynamics of simple metal-ligand ionic species in the gas phase. Using laser desorption coupled to Fourier transform mass spectrometry, we have successfully generated numerous highly unsaturated metal-ligand ions including bare metal carbenes, methyls, hydrides, nitrenes and amides. The combination of photodissociation, ion-molecule reactions and other techniques has made possible the determination of a wide variety of metal-ligand ion bond dissociation energies. Reactivity studies on these species reveal gas phase catalytic cycles including olefin homologation and  $\text{Fe}^+$  catalysed production of N—C bonds from  $\text{NH}_3$ , olefins and  $\text{N}_2\text{O}$ . General trends are observed in the reactions of  $\text{MOH}^+$ ,  $\text{MH}^+$ ,  $\text{MCH}_3^+$ , and  $\text{MNH}_2^+$  with alkanes;  $\text{MO}^+$  and  $\text{MS}^+$  with alkanes; and  $\text{MNH}^+$ ,  $\text{MCH}_2^+$  and  $\text{MO}^+$  with alkenes.

Research in gas-phase transition metal ion chemistry has undergone extremely rapid growth within the last ten years. Since the first observation of metal ion activation of saturated organic compounds by Allison, Freas and Ridge,<sup>1</sup> transition metal ions and small organometallic ions have been observed to be highly reactive and interesting species.<sup>2,3</sup> Catalysing the growth in the understanding of these chemical systems has been the evolution in the types of instrumental techniques which are being brought to bear on this problem, including ion-beam techniques,<sup>4</sup> Fourier transform mass spectrometry (FTMS)<sup>5,6</sup> and flowing afterglow.<sup>7</sup> In addition, new advances in sources, including laser desorption<sup>8</sup> and surface ionization,<sup>9</sup> and in structural techniques, including collision-induced dissociation (CID)<sup>10</sup> and photodissociation,<sup>11</sup> have begun to allow a more detailed study and understanding of the energetics and mechanisms of gas-phase transition metal ion systems.

In this review we discuss recent results from our laboratory on the chemistry, photochemistry and thermodynamics of a variety of gas-phase transition metal-ligand ions. The Experimental section will include a discussion of laser desorption for the production of bare metal ions, Fourier Transform mass spectrometry for trapping and detection, and

the methodology involved in collision-induced dissociation and photodissociation. The Discussion section will cover the methods used for preparing various highly unsaturated gas-phase metal-ligand ions, for determining ion structure and metal ion-ligand bond strengths by photodissociation, collision-induced dissociation and ion-molecule reaction studies, and for monitoring the gas-phase reactivity of metal ion-ligand species. Emerging trends in the last two areas will also be discussed.

### EXPERIMENTAL

The majority of the results described in this paper were obtained on a prototype Nicolet FTMS-1000 Fourier transform mass spectrometer equipped with a 5.2 cm cubic trapping cell situated between the poles of a Varian 15-in electromagnet maintained at 0.9 T. A diagram of this cell along with the laser desorption source is shown in Fig. 1. The transmitter plates have been replaced by 80% transmittance screens to allow light from an arc lamp into the cell for photodissociation experiments. The screens only decrease the detected ion current by a small amount. Photodissociation experiments on  $\text{Ni}(\text{Cp})(\text{NO})^+$  ( $\text{Cp}$  = cyclopentadienyl) were carried out on a conventional ion cyclotron resonance (ICR) spectrometer operated in the trapping mode. Some of the reactivity studies on the transition metal-amide complexes were performed on a newly

† Author to whom correspondence should be addressed.

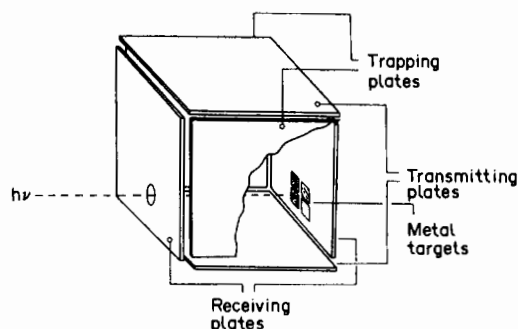


Fig. 1. Diagram of the FTMS trapping cell showing laser irradiation of metal targets for production of metal ions. Receiving plates have recently been replaced by 80% transmittance screens to permit irradiation of the cell with light from an arc lamp for photodissociation experiments.

acquired Nicolet FTMS-2000 Fourier transform mass spectrometer equipped with a differentially pumped dual cell configuration and a 3.0 T superconducting magnet.

The theory and instrumentation of ICR spectrometry and FTMS have been the subject of a number of recent reviews.<sup>12</sup> Briefly, an ion in a magnetic field is constrained to a circular orbit at a characteristic frequency proportional to the magnetic field and inversely proportional to the mass-to-charge ratio ( $m/z$ ) of the ion. If the ion is placed between two plates and a radio frequency (rf) field having the same frequency as the cyclotron frequency of the ion is applied to the plates, the ion will absorb energy and its velocity and radius of orbit will increase. This process is used in four main ways in our laboratory, (1) ion detection, (2) ion ejection, (3) collision-induced dissociation and (4) to study endothermic reactions.

In FTMS, detection is achieved by first exciting all of the ions to a larger orbit by applying what is termed an rf "chirp", a 0–2.5 MHz sweep in  $\sim 0.5$  ms.<sup>5</sup> This process also results in the ions moving in a coherent fashion, whereby each ion of the same  $m/z$  is in the same position in its orbit. The coherent motion of the ions induces an oscillating signal (image current) on the two receiving plates, see Fig.

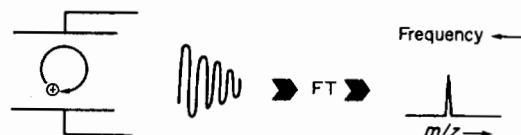


Fig. 2. Schematic depiction of the basic principles of FTMS. Coherent motion of ions in the cell produces an image current signal which is digitized and Fourier transformed. The result is a frequency or mass spectrum.

2. This signal is amplified, digitized and sent to the computer, where it is Fourier transformed producing the frequency domain or mass spectrum.

Ion ejection is a process where a high energy rf pulse excites selected ions to orbits larger than the size of the cell causing them to be annihilated (neutralized) on the cell plates.<sup>13</sup> Using this technique, an ion of specific  $m/z$  can be isolated from a whole population of ions by ejecting all of the other ions from the cell. This allows the selected ion to be further investigated without complications from the other ions.

Collision-induced dissociation (CID) also involves excitation of a selected ion at its cyclotron frequency by an rf pulse.<sup>10(b)</sup> The kinetically excited ion is then permitted to collide with a target gas, which is usually argon maintained at a static background pressure of  $\sim 1 \times 10^{-5}$  torr, after which it then undergoes fragmentation. The resulting fragment ions will often be diagnostic of the parent ion structure. However, rearrangements can occur prior to fragmentation and, thus, structures cannot always be unambiguously assigned from CID alone.

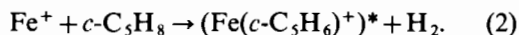
A technique similar in operation to CID can be used to synthesize ions by endothermic reactions.<sup>14</sup> A metal ion can be accelerated by an rf pulse at its cyclotron frequency in the presence of a reagent gas, as exemplified by reaction (1).



This allows formation of many metal–ligand ion species which cannot be prepared directly from thermalized ions by exothermic reactions (e.g.  $\text{ScH}^+$ ). Another advantage of this technique is that the threshold energy observed for process (1) yields a value for the bond energy of the product (e.g.  $D^0(\text{Sc}^+ - \text{H})$ ).

We have found pulsed laser desorption/ionization to be a particularly convenient method for generating virtually any metal ion from its pure metal rod or foil for study by FTMS. The fundamental (1064 nm) or frequency doubled (532 nm) output of a pulsed Quanta Ray Nd:YAG laser is used for production of metal ions. However, the process is essentially independent of the wavelength and simply requires sufficient laser power,  $\sim 10^8 \text{ W cm}^{-2}$ . Metal ions produced at high laser powers can have excess kinetic and electronic energy.<sup>15</sup> The photodissociation studies described here, therefore, were carried out using a high background pressure of buffer gas ( $\sim 1 \times 10^{-5}$  torr Ar) to permit the ions to undergo thermalizing collisions. Similar precautions were taken for the reaction studies and, in many cases, also involved reisolation of metal–ligand precursors after trapping  $\sim 250$ –500 ms

in  $\sim 1 \times 10^{-6}$  torr reagent gas. Non-composite pseudo first order decay kinetic plots indicated that these methods produce predominantly thermalized ions, although a small population of non-thermal ions cannot be completely ruled out. Another possible source of non-thermal ions is from exothermic reactions.<sup>16</sup> For example, when thermalized  $\text{Fe}^+$  reacts with cyclopentene to form  $\text{Fe}(\text{cyclopentadiene})^+$ , reaction (2), much of the reaction exothermicity ( $\sim 25\text{--}30 \text{ kcal mol}^{-1}$ ) remains with the ionic product.



The evidence for this is that the  $\text{Fe}(c\text{-C}_5\text{H}_8)^+$  product ion exhibits non-linear kinetics in its subsequent reactions. Trapping the  $(\text{Fe}(c\text{-C}_5\text{H}_8))^+$  in excess argon prior to reaction, however, cools the ion and yields linear kinetic plots.

Reagents used for formation of metal-ligand ions are admitted into the trapping cell through a General Valve Corp. series 9 pulsed solenoid valve. This allows the reagent to be pumped away prior to isolation of the appropriate metal-ligand ion, eliminating any complicating secondary reactions with that reagent during subsequent reaction sequences. A second pulsed valve has just been installed on our FTMS-1000 to permit even more control over the preparation of various reactant ions as exemplified below. Pulsed valve introduction of the reagents in FTMS has been previously discussed in detail.<sup>17</sup>

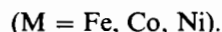
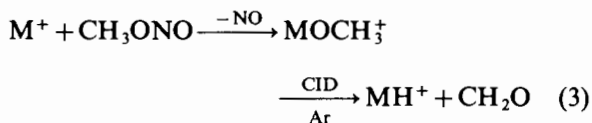
Photodissociation experiments are performed by irradiating the trapped (typically 2–10 s) ions with light from a 2.5 kW Hg–Xe arc lamp, used in conjunction with a Schoeffel 0.25 m monochromator set for 10 nm resolution. Photodissociation spectra are obtained by monitoring the appearance of ionic photoproducts as a function of the wavelength of light. Photodissociation onsets (the longest wavelength at which photoproducts are observed) are confirmed using white light and cut-off filters.

## DISCUSSION

### *Ion synthesis*

In our laboratory, gas-phase metal-ligand ions are prepared by one of three techniques, (1) from exothermic reactions,<sup>18</sup> (2) by CID of larger organometallic ions,<sup>19</sup> or (3) from endothermic reactions driven by kinetic excitation.<sup>14(b)</sup> Though (1) is the simplest and most commonly used method for the synthesis of ions, (2) and (3) allow generation of ions inaccessible by (1). For example, no reagent gas has yet been found to generate  $\text{MH}^+$  ( $\text{M} = \text{Fe}, \text{Co}, \text{Ni}$ ) in appreciable quantities directly by exo-

thermic reaction with  $\text{M}^+$ .

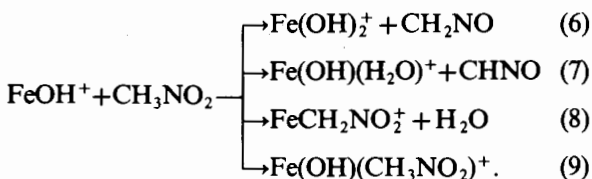


Collisional activation of  $\text{MOCH}_3^+$ , generated from methyl nitrite, however, produces  $\text{MH}^+$  in large abundance, [reaction (3)].<sup>19(a)</sup> As an example of method (3),  $\text{CrCH}_2^+$  can be generated by accelerating  $\text{Cr}^+$  into cyclopropane, reaction (4).<sup>16</sup>



$\text{CrCH}_2^+$  has not yet been observed as a reaction product from any exothermic reaction of  $\text{Cr}^+$ .

One difficulty often encountered in ion synthesis is secondary reactions with the parent neutral. For example,  $\text{FeOH}^+$ , formed in reaction (5), reacts further with  $\text{CH}_3\text{NO}_2$  as in reactions (6)–(9). These secondary reactions can obscure any reactivity studies which would subsequently be done on  $\text{FeOH}^+$  and renders photodissociation experiments impossible. This problem can be circumvented, however, by adding the initial reagent through a pulsed valve so, during the formation and isolation of the ion of interest (e.g.  $\text{FeOH}^+$ ), the reactant gas (e.g.  $\text{CH}_3\text{NO}_2$ ) is pumped away. The selected ion can then be permitted to react with a second reagent in the absence of the first.



A typical reaction sequence is shown in Fig. 3. Initially, the laser and the first pulsed valve are fired. Thus,  $\text{M}^+$  (in this case  $\text{Fe}^+$ ) is formed in the presence of a high pressure of the first reagent gas (in this case  $\text{N}_2\text{O}$ ). After an appropriate reaction period ( $\sim 400 \text{ ms}$ ), this reagent is pumped away and  $\text{ML}^+$  ( $\text{FeO}^+$  in this case) can be isolated by swept double resonance ejection pulses. At this point,  $\text{ML}^+$  can undergo reaction with a second reagent gas which is either present at a lower static background pressure ( $\sim 1 \times 10^{-6}$  torr), or is pulsed in by the second pulsed valve. One possibility is that the second reagent gas is required to prepare the desired reactant ion. For example, Fig. 3(d) shows formation of  $\text{FeNH}^+$  from the reaction of  $\text{FeO}^+$  with  $\text{NH}_3$ , which has been introduced via a second pulsed valve. After isolation, the ion of interest is reacted

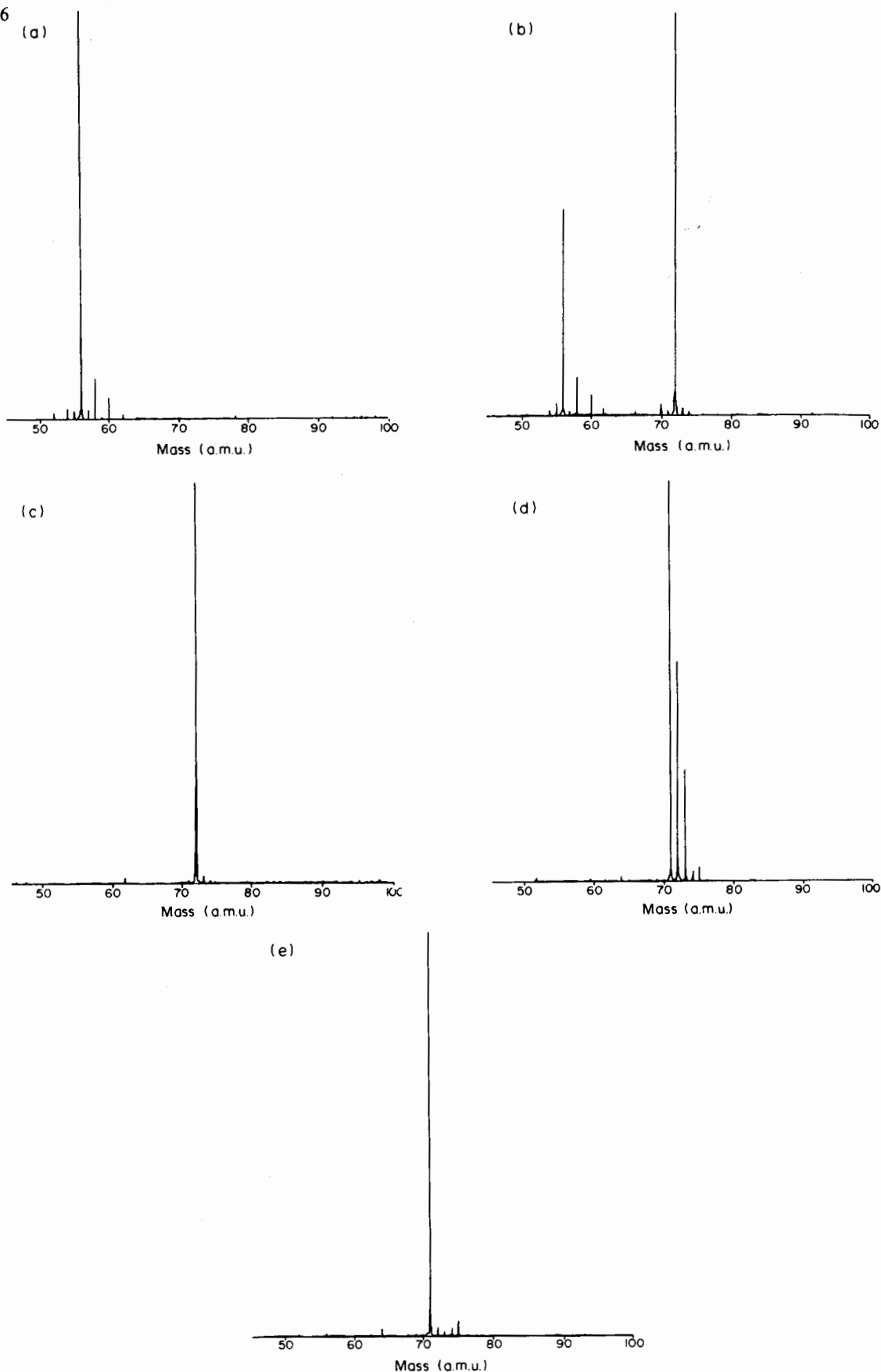


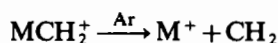
Fig. 3. Reaction sequence for gas-phase synthesis of  $\text{FeNH}^+$ . (a) Laser desorption of iron foil to produce  $\text{Fe}^+$  (peaks at  $m/z = 52$ ,  $58$  and  $60$  are due to impurities of Cr and Ni). (b) Reaction of  $\text{Fe}^+$  with  $\text{N}_2\text{O}$  to produce  $\text{FeO}^+$ . (c) Isolation of  $\text{FeO}^+$ . (d) Reaction of  $\text{FeO}^+$  with  $\text{NH}_3$ . (e) Isolation of  $\text{FeNH}^+$ .

with a background reagent gas. The final product ions may then be structurally interrogated by a variety of methods as discussed below.

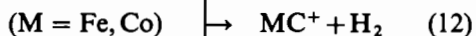
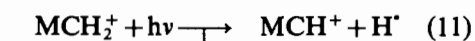
### Structural determination

In general a mass spectrum only reveals the mass-to-charge ratio of ions. In order to verify a proposed reaction mechanism, however, it is clearly necessary to determine both reactant and product ion structures. No one technique can definitively determine all ion structures, so a number of useful methods have been developed.

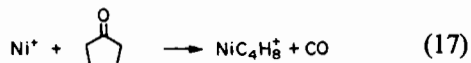
**Collision-induced dissociation and photodissociation.** Daughter ions produced upon fragmentation of ions will often be diagnostic for parent ion structure. Energy sufficient for dissociation can be put into an ion via energetic collisions (CID) or photons (photodissociation). These two techniques are very complementary, since they often produce significantly different dissociation products due to the nature of the excitation processes.<sup>20</sup> The low energy CID process is a multi-collision process and, as such, involves sequential addition of rotational and vibrational energy to the ion. This is in contrast to photodissociation where initially the ion undergoes an instantaneous electronic excitation. For example,  $MCH_2^+$  ( $M = Fe, Co$ ) undergoes CID via direct cleavage of  $CH_2$  to produce  $M^+$ , reaction (10), whereas photodissociation of  $MCH_2^+$  produces  $MCH^+$ ,  $MC^+$  and  $M^+$ , reactions (11)–(13).<sup>21</sup>



0–100 eV laboratory collision energy (10)



As a further illustration of these methods, photodissociation and collision-induced dissociation have been used to differentiate four  $NiC_4H_8^+$  isomers generated by reactions (14)–(17).<sup>20,22</sup>



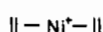
A comparison of the neutral losses upon collision-induced and photo-induced dissociation of these isomers is given in Table 1. The photodissociation

Table 1. Neutral losses from collision-induced dissociation and photodissociation of four  $NiC_4H_8^+$  isomers

Structure	Neutral losses	
	CID	PDS
$  -Ni^+-  $	$C_2H_4$ $C_4H_8$	$C_2H_4$ $C_4H_8$
$Ni^+-\text{isobutene}$	$C_4H_8$	$C_4H_8$ $CH_4$
$Ni^+-\text{1,3-butadiene}$	$H_2$ $C_4H_8$	$H_2$ $C_4H_8$ $C_2H_4$ $CH_3$
$Ni^+-\text{cyclopentadiene}$	$H_2$ $C_2H_4$ $C_4H_8$	$H_2$ $C_2H_4$ $C_4H_8$

spectra of these ions are shown in Fig. 4(a)–(d). Photodissociation has an additional advantage in structure differentiation in that differences in the photodissociation spectra, as well as different photoproducts, will often be observed. In addition, photodissociation spectra are characteristic of the ion structure *prior* to excitation and, therefore, are less susceptible than CID to misinterpretations due to rearrangements.

The proposed structures (I–IV) are shown for the



(I)

reaction 14



(II)

reaction 15



(III)

reaction 16

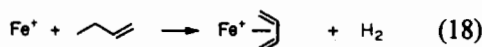


(IV)

reaction 17

products of reactions (14)–(17). As can be seen in Table 1, CID and photodissociation both can easily differentiate the four isomers. Also evident, as in the  $FeCH_2^+$  example discussed above, these two techniques can produce different fragments from the same ion. For example,  $Ni(\text{isobutene})^+$  undergoes photodissociation to lose  $CH_4$  as well as the entire ligand, whereas CID produces only direct cleavage of the isobutene. This is also interesting in light of an endothermic reaction study of  $Co^+$  with isobutene which showed formation of  $CoC_3H_4^+$  with loss of  $CH_4$ .<sup>23</sup>

Two isomers of  $FeC_4H_8^+$  have also been investigated by photodissociation.  $Fe(\text{butadiene})^+$  can be generated by reaction (18), and undergoes CID via direct cleavage of butadiene.



The photodissociation spectrum for this ion, which produces  $Fe^+$  exclusively, is shown in Fig. 5(a).

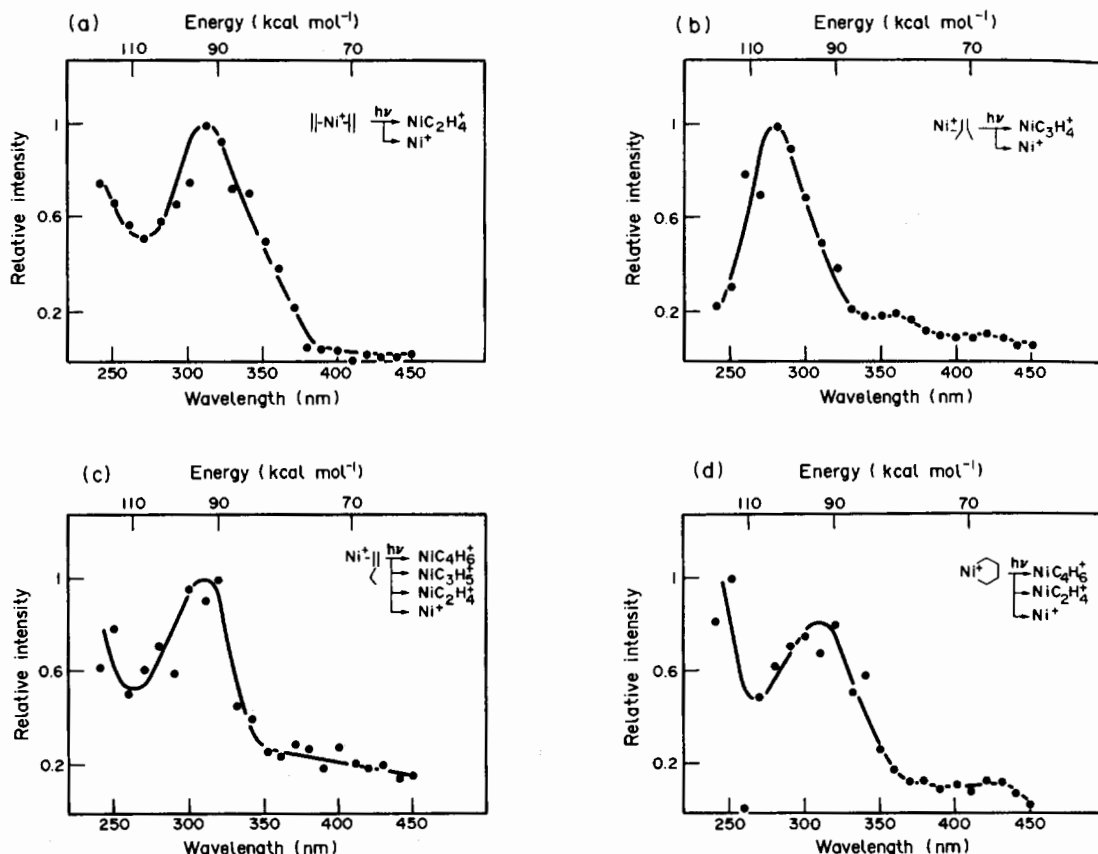
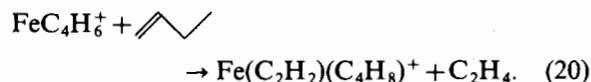


Fig. 4. Photodissociation spectra of four  $\text{NiC}_4\text{H}_8^+$  isomers. (a)  $\text{Ni}(\text{bis-ethylene})^+$ . (b)  $\text{Ni}(\text{isobutene})^+$ . (c)  $\text{Ni}(\text{1-butene})^+$ . (d)  $\text{Nickel metallacyclopentane}^+$ .

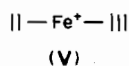
Electron impact ionization of trimethylene-methane(iron)tricarbonyl at 30 eV electron energy produces  $\text{FeC}_4\text{H}_6^+$ , reaction (19).



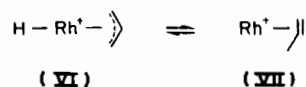
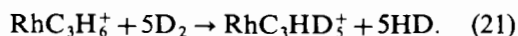
Collision-induced dissociation and photodissociation both yield loss of  $\text{C}_2\text{H}_2$ ,  $\text{C}_2\text{H}_4$  and  $\text{C}_4\text{H}_6$ . The photodissociation spectrum for this ion is shown in Fig. 5(b). These observations, along with the observation of the displacement of  $\text{C}_2\text{H}_4$  by 1-butene, reaction (20), indicate the ion produced in reaction (19) may have rearranged upon electron impact to an iron-ethylene-acetylene complex, structure (V).



In any event CID and photodissociation provide clear evidence for the existence of at least two  $\text{FeC}_4\text{H}_6^+$  isomers.



*Ion-molecule reactions.* In analogy to solution phase qualitative analysis, ion-molecule reaction chemistry can be used to differentiate isomers, since they will generally display different reactivities. The main two methods used in this category are H/D exchange reactions<sup>24</sup> and ligand displacement reactions. H/D exchange is performed by trapping a selected ion in a static background of a deuterating reagent such as  $\text{D}_2$ ,  $\text{C}_2\text{D}_4$ , or  $\text{C}_3\text{D}_6$ . The number of exchangeable H atoms will be characteristic of the ionic structure. For example,  $\text{RhC}_3\text{H}_5^+$  reacts with  $\text{D}_2$  to exchange 5 H atoms, reaction (21), providing evidence for a rapid equilibrium between the hydrido-allyl structure (VI) and the propene structure (VII).<sup>24(a)</sup>



Another interesting example involves the reactions of  $\text{Fe}^+$ ,  $\text{Co}^+$  and  $\text{Ni}^+$  with cyclobutanone to

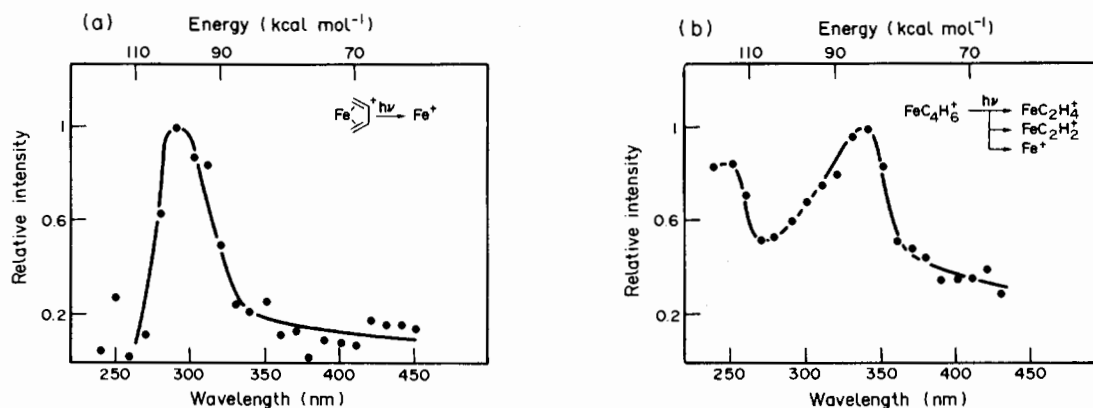
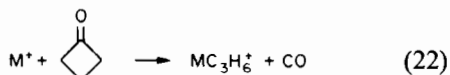
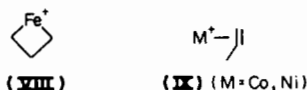


Fig. 5. Photodissociation spectra of two  $\text{FeC}_4\text{H}_6^+$  isomers. (a)  $\text{Fe}(\text{butadiene})^+$ . (b)  $\text{FeC}_4\text{H}_6^+$  generated from electron impact on trimethylenemethane(iron)tricarboxyl.

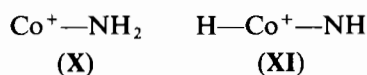
generate  $\text{MC}_3\text{H}_6^+$ , reaction (22).<sup>25</sup>



Using  $\text{C}_2\text{D}_4$  as the deuterating reagent, it was found that  $\text{FeC}_3\text{H}_6^+$  generated in this way has a stable metallocyclobutane structure (**VIII**), while  $\text{CoC}_3\text{H}_6^+$  and  $\text{NiC}_3\text{H}_6^+$  apparently isomerize to the propene structure (**IX**). The implications of these results are discussed by the authors, as well as the differentiation of other isomeric ions.



Ligand displacement, as shown in reaction (20), will produce displacement of a more weakly bound ligand by a more strongly bound ligand. For instance, benzene will displace an H atom from  $\text{Co}^+$ .  $\text{CoNH}_2^+$  reacts with benzene to displace  $\text{NH}_2$ , exclusively, suggesting that  $\text{CoNH}_2^+$  has an amide structure (**X**) and not a hydrido-nitrene structure, (**XI**).<sup>26</sup>



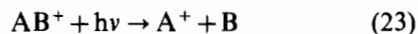
Another prime example by Beauchamp and coworkers was the differentiation of structures **I** and **IV** using  $\text{HCN}$  as the reagent gas.<sup>27</sup> In this case structure **I** was observed to undergo the sequential displacement of one and then two molecules of  $\text{C}_2\text{H}_4$  with  $\text{HCN}$ , while structure **IV** is completely unreactive with  $\text{HCN}$ . This result provided significant evidence for the notion that bare metal ions can undergo C—C insertion in alkanes. An extension of this work was performed in our laboratory on a variety of  $\text{Fe}^+$ ,  $\text{Co}^+$  and  $\text{Ni}^+$  olefin complexes.<sup>3(d),22</sup>

### Techniques for the determination of metal-ligand bond strengths

The determination of absolute bond energies for metal-ligand systems is of primary importance to organometallic chemistry. Bond energies aid in understanding structure and bonding as well as in determining the feasibility of various reaction mechanisms.

Several complementary techniques have been developed for the determination of metal-ligand bond energies of ionic species in the gas phase including: (1) appearance potentials,<sup>28</sup> (2) thermal ion-molecule reactions,<sup>18(b),c</sup> (3) endothermic reaction thresholds,<sup>4,14</sup> (4) ligand equilibria,<sup>29,30</sup> (5) photodissociation thresholds<sup>20,31</sup> and (6) competitive CID.<sup>32</sup> Methods (2) and (5) are the main techniques used in our laboratory and are, therefore, described in the greatest detail below.

**Photodissociation.** Photodissociation, process (23),



is controlled by three factors: (a) the ion must first absorb a photon, (b) the photon energy must exceed the enthalpy for process (23) and (c) the quantum yield for photodissociation must be greater than zero. Thus, photodissociation cut-offs can be attributed to either spectroscopic or thermodynamic factors. If the first allowed electronic state lies above the energy for process (23), then the photodissociation threshold will be determined by spectroscopic factors (see Fig. 6) and yield only an upper limit for the enthalpy of process (23). If an allowed electronic state lies at the same energy as process (23), or a high density of states lies in this energy range, then the threshold will be determined by thermodynamic factors and will yield an absolute



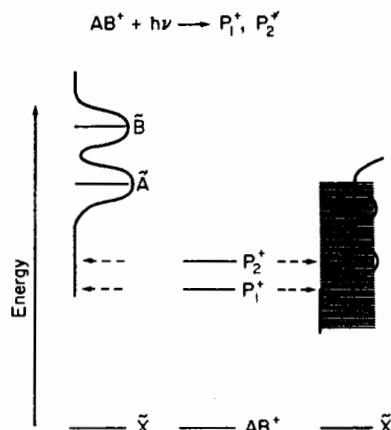


Fig. 6. Energy level diagram showing cases where photodissociation thresholds are determined by spectroscopic factors, due to a low density of low-lying electronic states (left) and thresholds determined by thermodynamic factors due to a high density of low-lying electronic states (right).

value for the bond energy. In general, photodissociation onsets of organic ions tend to be spectroscopically determined, while data from our laboratory suggest that many metal ion species yield thermodynamic thresholds. Due to the presence of the metal, a high density of low-lying electronic states results in a broad absorption in the vicinity of the bond dissociation energy. For example, the photoappearance spectrum for  $\text{Fe}^+$ , obtained by irradiating  $\text{FeO}^+$ , is shown in Fig. 7. The threshold at  $420 \pm 10$  nm implies  $D^0(\text{Fe}^+ - \text{O}) = 68 \pm 5$  kcal mol $^{-1}$ , in excellent agreement with a value of  $D^0(\text{Fe}^+ - \text{O}) = 68 \pm 3$  kcal mol $^{-1}$  obtained in an ion-beam study by Beauchamp *et al.*<sup>33</sup> This clearly indicates that the threshold is due to the ther-

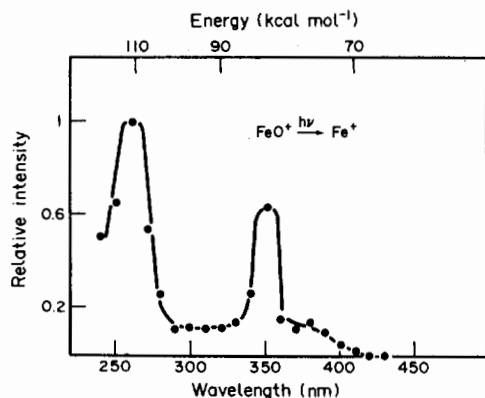
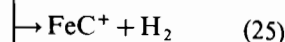
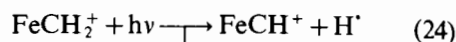


Fig. 7. Photodissociation spectrum of  $\text{FeO}^+$  with the threshold at 420 nm indicating  $D^0(\text{Fe}^+ - \text{O}) = 68 \pm 5$  kcal mol $^{-1}$ .

modynamics of the photodissociation process, involving a simple bond cleavage to produce ground state products.

Often, multiple products are observed from photodissociation. For example,  $\text{FeCH}_2^+$  undergoes photodissociation in the vis-UV region to give three product ions, reactions (24)–(26).<sup>21</sup>



For this type of situation, each photoproduct can be measured as a function of wavelength. If rapid internal conversion to a vibrationally excited ground state occurs with subsequent randomization of the energy, then thresholds for higher energy photoproducts can also yield absolute thermodynamic values. Photoappearance spectra for reactions (25) and (26) are shown in Fig. 8. Photodissociation thresholds for  $\text{FeCH}^+$  and  $\text{FeC}^+$  imply  $D^0(\text{Fe}^+ - \text{CH}) = 101 \pm 5$  kcal mol $^{-1}$  and  $D^0(\text{Fe}^+ - \text{C}) = 94 \pm 5$  kcal mol $^{-1}$ , in reasonable agreement with  $D^0(\text{Fe}^+ - \text{CH}) = 115 \pm 20$  kcal mol $^{-1}$ <sup>34</sup> and  $D^0(\text{Fe}^+ - \text{C}) \sim 89$  kcal mol $^{-1}$ <sup>34</sup> obtained from ion-beam experiments. These results indicate that, for  $\text{FeCH}_2^+$  at least, the thresholds for higher energy products can be attributed to thermodynamic factors.

**Ion-molecule reactions.** In the gas phase, the attraction between an ion and the permanent and/or induced dipole of the neutral is long range and in general leads to an interaction with little or no activation barrier. Thus, if an ion-molecule reaction is observed in the gas phase, the free energy of reaction (27) can be assumed to be negative.

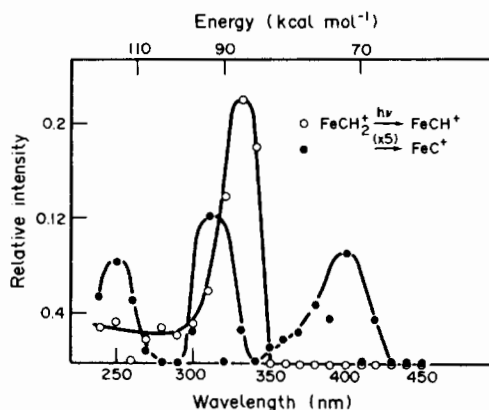
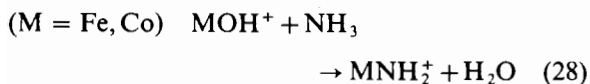


Fig. 8. Photoappearance spectra for  $\text{FeCH}^+$  and  $\text{FeC}^+$  produced upon photodissociation of  $\text{FeCH}_2^+$ .

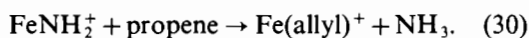
Furthermore, since entropy effects are often negligible, the enthalpy of the reaction can also be assumed to be negative. Thus, limits on the heats of formation can be derived from the observation of a reaction. For example, from the observation of reaction (28)



and using the known heats of formation for  $\text{H}_2\text{O}$ ,  $\text{NH}_3$  and  $\text{MOH}^+$ ,  $\Delta H_f(\text{MNH}_2^+)$  can be derived from eq. (29).

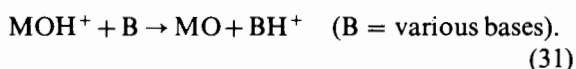
$$\Delta H_f(\text{MNH}_2^+) < \Delta H_f(\text{NH}_3) + \Delta H_f(\text{MOH}^+) - \Delta H_f(\text{H}_2\text{O}). \quad (29)$$

Then, from  $\Delta H_f(\text{MNH}_2^+)$ , lower limits for the bond energies of  $D^0(\text{Co}^+ - \text{NH}_2) > 56 \pm 3 \text{ kcal mol}^{-1}$  and  $D^0(\text{Fe}^+ - \text{NH}_2) > 58 \pm 3 \text{ kcal mol}^{-1}$  are obtained.<sup>26</sup> Upper limits can also be derived using a similar procedure.



Reaction (30), for example, indicates  $D^0(\text{Fe}^+ - \text{NH}_2) < 72 \pm 7 \text{ kcal mol}^{-1}$ , using previously reported heats of formation for the other species. Finally, from the upper and lower brackets, a value of  $D^0(\text{Fe}^+ - \text{NH}_2) = 67 \pm 12 \text{ kcal mol}^{-1}$  is obtained.

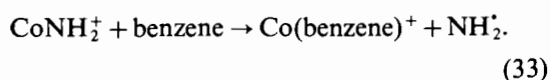
Two important ion-molecule reactions frequently used to determine thermochemistry are proton transfer<sup>31</sup> and ligand displacement reactions.<sup>19(b)</sup> An example of the former is the reaction of  $\text{MOH}^+$  ( $M = \text{Fe, Co}$ ) with various bases, reaction (31):



For  $\text{CoOH}^+$ , proton transfer is observed with pyridine or stronger bases but is not observed with 1-propylamine or weaker bases indicating  $\text{PA}(\text{pyridine}) > \text{PA}(\text{CoO}) > \text{PA}(\text{1-propylamine})$ . Using this result in eq. (32) yields  $D^0(\text{Co}^+ - \text{OH}) = 71 \pm 6 \text{ kcal mol}^{-1}$ , in good agreement with  $D^0(\text{Co}^+ - \text{OH}) = 71 \pm 3 \text{ kcal mol}^{-1}$  obtained from photodissociation.<sup>31</sup>

$$\Delta H_f(\text{MOH}^+) = \Delta H_f(\text{MO}) + \Delta H_f(\text{H}^+) - \text{PA}(\text{MO}). \quad (32)$$

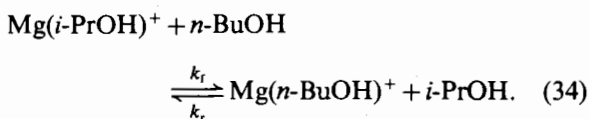
Ligand displacement reactions can also be used to determine bond energy limits, as in reaction (33), which indicates  $68 \pm 5 \text{ kcal mol}^{-1} = D^0(\text{Co}^+ - \text{benzene}) > D^0(\text{Co}^+ - \text{NH}_2)$ .<sup>26</sup>



Thermodynamic information derived from ion-molecule reactions must clearly be viewed with caution. Absence of a reaction may be due to kinetic and not thermodynamic factors. Competing reaction channels may prevent observation of all exothermic pathways. Also, ion-molecule reactions which are slightly ( $1-3 \text{ kcal mol}^{-1}$ ) endothermic can still be observed, though they will proceed very slowly ( $k^{\text{II}} < 5\%$  of Langevin rate).<sup>35,36</sup> This is because the equilibrium is being driven by an infinite excess of one reagent. For example, in the  $\text{CoOH}^+$  case, reaction (31), no  $\text{CoO}$  is present to be reprotonated by  $\text{BH}^+$ , so thermoneutral or slightly endothermic reactions can be observed. Finally, as discussed earlier, care must be taken to ensure that the reactant ions are thermalized. Thus, it is important to have other techniques to verify thermochemical values.

*Other techniques.* The most common method used to corroborate the thermodynamic results obtained by photodissociation and ion-molecule reactions is competitive CID. This technique was first developed by Cooks and coworkers to obtain proton affinity information,<sup>32</sup> but can be generalized to other cation affinities (including metal ions) and anion affinities. In particular, a metal cation centre which contains two ligands will undergo collisional activation via competitive loss of the ligands. In general, loss of the more weakly bound ligand should be favoured in the dissociation process. For example, CID of  $\text{Mg}(\text{EtOH})(n\text{-PrOH})^+$  favours production of  $\text{Mg}(n\text{-PrOH})^+$  over  $\text{Mg}(\text{EtOH})^+$  indicating  $D^0(\text{Mg}^+ - n\text{-PrOH}) > D^0(\text{Mg}^+ - \text{EtOH})$ .<sup>37</sup> A second example is the observation that CID of  $\text{CoC}_6\text{H}_7^+$  yields  $\text{CoC}_6\text{H}_6^+$  indicating  $52 \pm 4 \text{ kcal mol}^{-1} = D^0(\text{Co}^+ - \text{H}) < D^0(\text{Co}^+ - \text{benzene})$ .<sup>18(b)</sup> One difficulty with this approach has recently been suggested. Restrictions on the change in angular momentum during the dissociation process may affect the relative rates of dissociation and hence the product distributions, regardless of the relative bond dissociation energies.<sup>38</sup>

Another powerful approach, which yields accurate relative bond energies, is to determine the equilibrium constant for ligand displacement, as exemplified by reaction (34).



This value can be obtained from the ratio of the partial pressures of the ligands in the cell and from the ratio of the steady-state ion populations at equilibrium.  $K_{\text{eq}}$  can also be obtained from the relation

$K_{eq} = k_f/k_r$ , by measuring the forward and reverse rate constants for reaction (34) in two separate experiments. From  $\Delta G = -RT \ln K$  and again assuming  $\Delta S$  is small, an accurate value ( $\pm 0.1$  kcal mol<sup>-1</sup>) for the difference in binding energies for the two ligands can be obtained. Table 2 shows the ladder of relative bond strengths for various oxygen bases bound to Mg<sup>+</sup> obtained by ligand exchange equilibria.<sup>37</sup> The absolute bond energies shown in the table were derived from photodissociation experiments.

Finally, endothermic reactions can be used to determine metal-ligand bond strengths. For example, translationally excited Co<sup>+</sup> reacts with ethane as in reaction (35).



The threshold energy for production of CoCH<sub>3</sub><sup>+</sup> of  $1.82 \pm 0.62$  eV gives the endothermicity for the reaction.<sup>14(b)</sup> From the known heats of formation for the other species,  $D^0(\text{Co}^+ - \text{CH}_3) = 46 \pm 14$  kcal mol<sup>-1</sup> was obtained, in comparison to  $D^0(\text{Co}^+ - \text{CH}_3) = 61 \pm 4$  kcal mol<sup>-1</sup> obtained from an ion-beam experiment<sup>39</sup> and  $D^0(\text{Co}^+ - \text{CH}_3) = 57 \pm 7$

kcal mol<sup>-1</sup> determined by photodissociation.<sup>20</sup> Results from measuring endothermic thresholds using FTMS must be viewed with caution, however, since the spread in translational energies in the instrument is not well characterized and the signal-to-noise is low near threshold. In addition, the elimination of barriers, which normally accompanies thermal reactions due to the formation of an intimate ion-induced dipole collision complex, may not occur at higher energies where scattering type collisions occur.

#### Summary of thermodynamic results

As discussed above for photodissociation and ion-molecule reactions, there are assumptions made for every technique and spectroscopic, kinetic and other factors may be the controlling influence as opposed to thermodynamic factors. For this reason, it is essential that each thermodynamic value be checked by as many techniques as possible. Table 3 lists the results obtained in our laboratory by photodissociation, ion-molecule reactions,

Table 2. Relative and absolute gas phase ligand binding energies to Mg<sup>+</sup> for various organic molecules<sup>a</sup>

Ligand (L)	Measured $\Delta G_{\text{exchange}}^b$	$D^0(\text{Mg}^+ - \text{L})$	
		Rel. <sup>c</sup>	Abs. <sup>d</sup>
MeCOEt	1.24	7.64	68
Me <sub>2</sub> CO	1.05	6.40	67
THF <sup>e</sup>	0.23	5.41	66
Et <sub>2</sub> O	0.52	5.16	66
<i>n</i> -PrCHO	0.86	4.60	66
<i>n</i> -BuOH	1.76	3.87	65
EtCHO	0.72	3.67	65
<i>i</i> -PrOH		3.59	65
<i>n</i> -PrOH	0.68	2.95	64
MeCHO	0.52	2.28	63
EtOH	1.77	1.77	63
MeOH		0.00	61

<sup>a</sup> All data are in kcal mol<sup>-1</sup>.

<sup>b</sup> For the equilibrium reaction (34) in text.

<sup>c</sup> Values ( $\pm 0.2$  kcal mol<sup>-1</sup>) are relative to  $D^0(\text{Mg}^+ - \text{MeOH}) = 0.00$  kcal mol<sup>-1</sup>.

<sup>d</sup> Absolute values ( $\pm 5$  kcal mol<sup>-1</sup>) assigned from photodissociation results, see text.

<sup>e</sup> Tetrahydrofuran.

Table 3. Bond dissociation energies for various gaseous ions obtained by various methods (see text). All values in kcal mol<sup>-1</sup>

Bond	PDS	I—M reactions	Competitive CID	Endothermic reactions	Ref.	Lit.	Ref.
Co <sup>+</sup> —CH <sub>2</sub>	84 ± 5			81 ± 7	14(b), 21	84 ± 7	57
Co <sup>+</sup> —CH	100 ± 5				21		
Co <sup>+</sup> —C	90 ± 5				21	98	34
Fe <sup>+</sup> —CH <sub>2</sub>	82 ± 5				21	96 ± 5	58
Fe <sup>+</sup> —CH	101 ± 5				21	115 ± 20	34
Fe <sup>+</sup> —C	94 ± 5				21	89	34
Rh <sup>+</sup> —CH <sub>2</sub>	89 ± 5	94 ± 5			49, 50		
Rh <sup>+</sup> —CH	102 ± 7				50		
Rh <sup>+</sup> —C	> 120	164 ± 16			50, 59		
La <sup>+</sup> —CH <sub>2</sub>	106 ± 5	> 93			50, 54		
La <sup>+</sup> —CH	125 ± 8				50		
La <sup>+</sup> —C	102 ± 8				50		
Nb <sup>+</sup> —CH <sub>2</sub>	109 ± 5	112 ± 5			50, 51		
Nb <sup>+</sup> —CH	145 ± 8				50		
Nb <sup>+</sup> —C	> 88				50		
Fe <sup>+</sup> —S	65 ± 5	74 > x > 59			48		
Co <sup>+</sup> —S	62 ± 5	74 > x > 59			48		
Ni <sup>+</sup> —S	60 ± 5				48		
Fe <sup>+</sup> —CH <sub>3</sub>	65 ± 5				20	69 ± 5	60
Co <sup>+</sup> —CH <sub>3</sub>	57 ± 7			46 ± 14	14(b), 20	61 ± 4	33
Co <sup>+</sup> —CH <sub>3</sub> CN	> 61 ± 4				19(b)		
Fe <sup>+</sup> —O	68 ± 5				20	68 ± 3	33
NiCp <sup>+</sup> —NO	< 43 ± 3				56	41.9 ± 1	61
Fe <sub>2</sub> <sup>+</sup> —H				52 ± 16	14(b)		
V <sup>+</sup> —C <sub>6</sub> H <sub>6</sub>	62 ± 5	> 49			20, 47		
VC <sub>6</sub> H <sub>6</sub> <sup>+</sup> —C <sub>6</sub> H <sub>6</sub>	57 ± 7				20		
Co <sup>+</sup> —C <sub>6</sub> H <sub>6</sub>	68 ± 5	66 ± 7	> 48		18(b), 19(b), 20		
Fe <sup>+</sup> —C <sub>6</sub> H <sub>6</sub>	55 ± 5				20		
Fe <sup>+</sup> —H			55 ± 5		18(b)	47 ± 4, 60 ± 3	62, 63
Ni <sup>+</sup> —C <sub>3</sub> H <sub>5</sub>	< 60	> 55			20		
Fe <sup>+</sup> —butadiene	48 ± 5	60 > x > 45			20		
Ni <sup>+</sup> —2C <sub>2</sub> H <sub>4</sub>	80 ± 5	74 ± 2			20		
Rh <sup>+</sup> —C <sub>6</sub> H <sub>6</sub>	66 ± 7	> 49			16, 24(a)		
Nb <sup>+</sup> —C <sub>6</sub> H <sub>6</sub>	66 ± 7	> 60	< 73		16		
Co <sup>+</sup> —OH	71 ± 3	71 ± 6			31		
Fe <sup>+</sup> —OH	73 ± 3	77 ± 6			31		
Fe <sup>+</sup> —(c-C <sub>3</sub> H <sub>5</sub> )	51 ± 5				16		
Co <sup>+</sup> —Cp		85 ± 10			53		
CoCp <sup>+</sup> —Cp		118 ± 10			53		
CoCp <sup>+</sup> —butadiene		> 57			53		
Co <sup>+</sup> —butadiene		< 52			18(a)		
Co <sup>+</sup> —C <sub>3</sub> H <sub>5</sub>		> 72			18(a)		
Co—CH <sub>4</sub>		49 ± 11			18(a)		
Co <sup>+</sup> —toluene			> 48		44		
Fe <sup>+</sup> —Cp		> 66			18(b)		
Fe <sup>+</sup> —NH <sub>2</sub>		67 ± 12			26		
Co <sup>+</sup> —NH <sub>2</sub>		65 ± 8			26		
V <sup>+</sup> —NH		100 ± 7			16		
VN—H <sup>+</sup>		220 ± 7			16		
V—N		110 ± 10			16		
Fe <sup>+</sup> —NH	61 ± 5	54 ± 14			16		
FeO—H <sup>+</sup>		219 ± 5			31		
CoO—H <sup>+</sup>		219 ± 5			31		

PDS = photodissociation.

I—M Reactions = ion-molecule reactions.

endothermic reaction thresholds and competitive CID. These values are also compared where available with other literature values, primarily from ion-beam experiments, and good agreement is observed in general.

Of particular note are the high bond strengths of  $MNH_2^+$  ( $M = Fe, Co$ ). Primary amide complexes of later transition metals have not been observed in condensed phase, which has been attributed to the unfavourable nitrogen  $p$ /metal  $d$  interaction which would presumably make the  $M-N$  bond extremely weak.<sup>40</sup> Furthermore, earlier gas-phase studies had also suggested the possibility of an extremely weak  $Co^+-NH_2$  bond ( $< 19 \text{ kcal mol}^{-1}$ ).<sup>41</sup>  $CH_3CN$  displaces  $CH_3$  from  $CoCH_3^+$  but does not displace  $NH_2$  from  $CoNH_2^+$  in accordance with the bond energies in Table 3 indicating  $D^0(Co^+-NH_2) > D^0(Co^+-CH_3)$ . This trend is the opposite of that observed in solution studies.<sup>42</sup>

An interesting correlation for the determination of bond energy/bond order relationships has recently

been suggested by Aristov and Armentrout.<sup>43</sup> Plots of  $M^+-L$  bond energies versus those of the corresponding carbon analogues are observed to be linear with distinct regions appearing which correspond to single, double and triple bonds. Using the values from Table 3, plots for  $Fe^+$ ,  $Co^+$ ,  $Rh^+$ ,  $Nb^+$ ,  $La^+$  and  $V^+$  are shown in Fig. 9(a)–(d). Single bond regions are defined by  $M^+-H$  bonds and double bonds are defined by  $M^+-CH_2$  bonds, in line with recent theoretical results. One immediate feature of these plots is the propensity of early transition metal ions to form multiple bonds to oxygen and nitrogen containing ligands, in contrast to their later transition metal counterparts which form primarily single bonds. This is believed to be due to the empty  $d$ -orbitals in the early transition metals which are available for multiple bonding.

Interestingly, this type of correlation is also observed for the neutral  $V-L$  species (see Fig. 10). Thermochemical values for  $VN$  were derived using reactions (36)–(38) and the other data used were

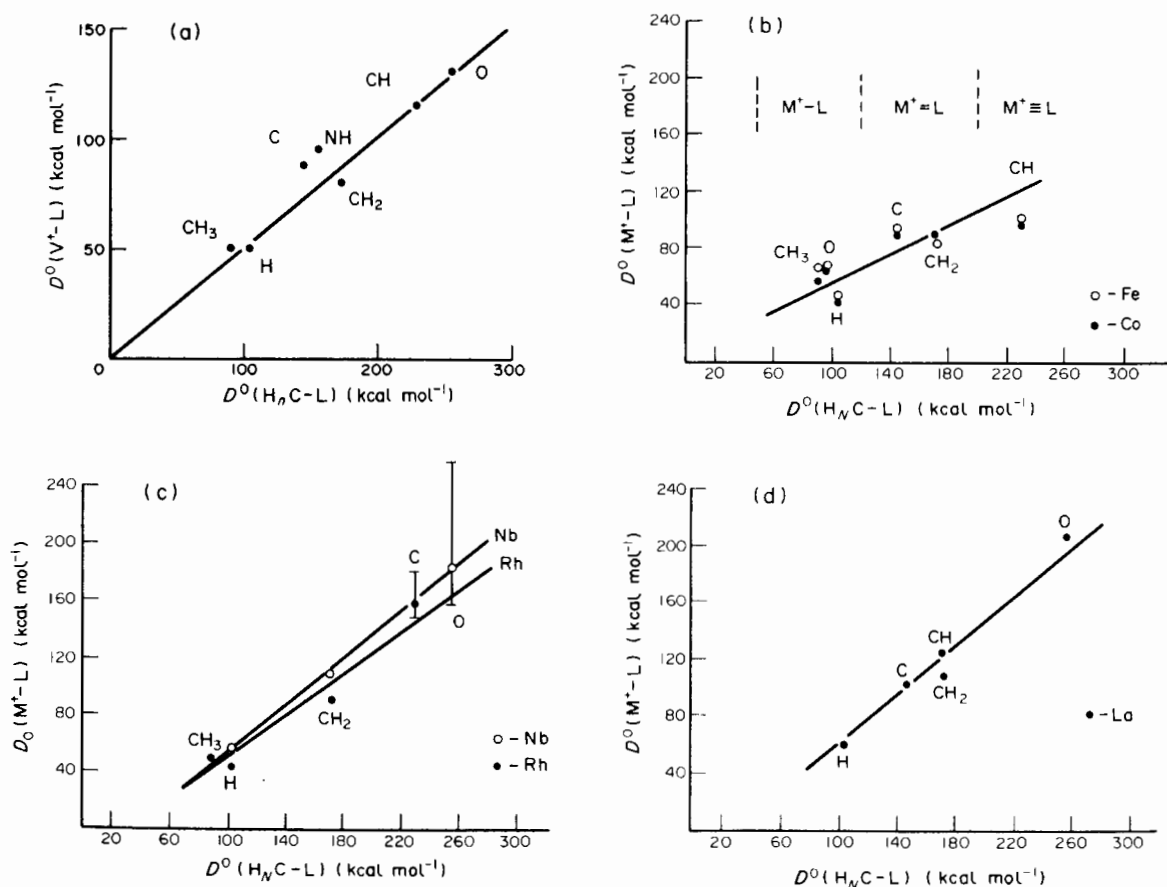


Fig. 9. Correlation of metal ion-ligand bond dissociation energies ( $D^0(M^+-A)$ ) with the corresponding carbon analogues  $D^0(H_N C-A)$ . (a)  $V^+-L$ . (b)  $Fe^+-L$ ,  $Co^+-L$ . (c)  $Nb^+-L$ ,  $Rh^+-L$ . (d)  $La^+-L$ .

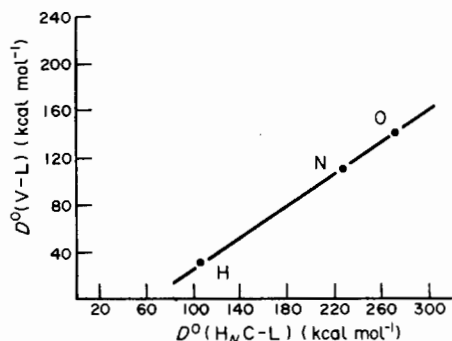
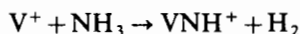
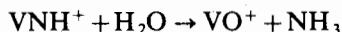


Fig. 10. Correlation of the neutral vanadium-ligand bond dissociation energies with the corresponding carbon analogues.

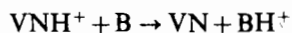
taken from the literature.



$$\text{implies } D^0(\text{V}^+-\text{NH}) > 93 \text{ kcal mol}^{-1} \quad (36)$$



$$\text{implies } D^0(\text{V}^+-\text{NH}) < 107 \text{ kcal mol}^{-1} \quad (37)$$



$$\text{implies } PA(\text{VN}) = 220 \pm 6 \text{ kcal mol}^{-1}. \quad (38)$$

These plots must be viewed with caution, though. The idea that  $\text{M}^+-\text{L}$  bond energies should correlate with their organic analogues is clearly an oversimplification, as multiple bonds in condensed phase inorganic species are often weaker than single bonds.

### Reactivity of $\text{ML}^+$

In this section we will discuss the reactivity of various ligated atomic metal ions ( $\text{M} = \text{Fe}, \text{Co}, \text{Ni}, \text{V}, \text{Rh}, \text{Nb}, \text{La}$ ;  $\text{L} = \text{H}, \text{CH}_3, \text{NH}_2, \text{OH}, \text{O}, \text{S}, \text{NH}, \text{CH}_2$ ,  $\pi$ -type ligands) with various alkanes and alkenes. First a discussion of the reactivity of bare atomic metal ions will be useful for comparison.

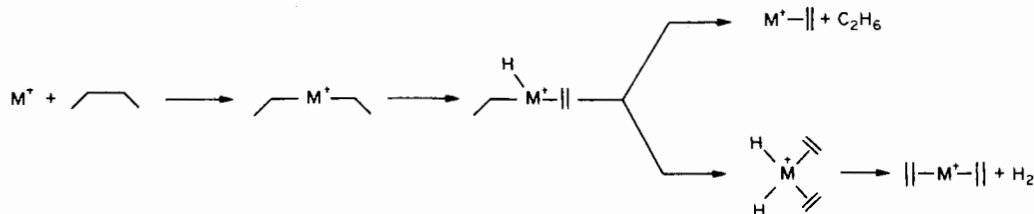
There have been numerous studies of the reactivity of atomic metal ions with organic

compounds,<sup>2</sup> making possible a good understanding of the driving force behind their reactivity. By far the most heavily studied metal ions have been  $\text{Fe}^+$ ,  $\text{Co}^+$  and  $\text{Ni}^+$ . These metal ions react with hydrocarbons predominantly by attacking the C—C bonds, as exemplified by the proposed mechanism in Scheme 1. This is in contrast to solution where organometallic complexes of these metals only activate C—H bonds. One explanation for the gas phase behaviour is that C—C bond insertion is more thermodynamically favourable than C—H insertion, since C—C bonds are weaker than C—H bonds and  $\text{M}^+$ -alkyl bonds are stronger than  $\text{M}^+-\text{H}$  bonds.

In contrast to the reactivity of the first row groups 8–10 metal ions, the other metal ions studied to date have been observed to predominantly activate C—H bonds in hydrocarbons. A survey of the reactivity of  $\text{Fe}^+$ ,  $\text{Co}^+$ ,  $\text{Ti}^+$ ,  $\text{Rh}^+$ ,  $\text{Ta}^+$ ,  $\text{Y}^+$  and  $\text{Nb}^+$  with methane through propane is shown in Table 4.

The discussions of  $\text{ML}^+$  reactivity will be broken up into groups with similar reactivity.  $\text{L} = \text{H}, \text{CH}_3, \text{NH}_2, \text{OH}$ ; where predominant formation of metal-alkyl and metal-allyl occurs upon the loss of the original ligand.  $\text{L} = \text{O}, \text{S}$ ; where the loss of  $\text{H}_2\text{O}$  and  $\text{H}_2\text{S}$  occurs with formation of an activated  $\text{M}^+$ -alkene complex which further decomposes.  $\text{L} = \text{CH}_2, \text{NH}$ ; where formation of a four-centred intermediate leads to catalytic homologation reactions, and lastly  $\text{L} =$  various  $\pi$ -type ligands.

$\text{L} = \text{H}, \text{CH}_3, \text{OH}, \text{NH}_2$ . The reactivity of these ligands is governed by the expected behaviour of a singly bonded-sigma bound species.<sup>16,18(a)(b),19(a),44</sup> One of the main reaction pathways with small hydrocarbons is shown in Scheme 2. Again, oxidative addition is the first step of the reaction. For  $\text{FeL}^+$ ,  $\text{CoL}^+$  and  $\text{NiL}^+$  it is interesting to note that initial insertion occurs across C—H bonds. This is in contrast to the bare atomic metal species which almost exclusively attack C—C bonds. An increased preference for C—H bond activation relative to C—C bond activation is observed for all ligated  $\text{Fe}^+$ ,  $\text{Co}^+$  and  $\text{Ni}^+$  species studied to date. After the initial oxidative addition, rapid reductive



Scheme 1.

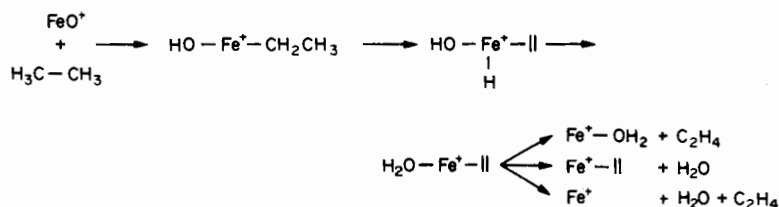


Table 5. Product distributions for the reactions of  $ML^+$  with various alkanes ( $L = H, CH_3, OH, NH_2$ )

Reactant	Products	FeD <sup>+</sup>	CoD <sup>+</sup>	NiD <sup>+</sup>	FeCH <sub>3</sub> <sup>+</sup>	CoCH <sub>3</sub> <sup>+</sup>	FeOH <sup>+</sup>	CoOH <sup>+</sup>	FeNH <sub>2</sub> <sup>+</sup>
CH <sub>4</sub>	MH <sup>+</sup> + CH <sub>3</sub> D MCH <sub>3</sub> <sup>+</sup> + HL	NR	NR	20 80	NR	NR	NR	NR	NR
C <sub>2</sub> H <sub>6</sub>	MC <sub>2</sub> H <sub>5</sub> <sup>+</sup> + HL	NR	100	100	NR	NR	NR	NR	NR
C <sub>3</sub> H <sub>8</sub>	MC <sub>3</sub> H <sub>7</sub> <sup>+</sup> + HL MC <sub>3</sub> H <sub>5</sub> <sup>+</sup> + HL + H <sub>2</sub> MC <sub>3</sub> H <sub>6</sub> L <sup>+</sup> + H <sub>2</sub> C <sub>3</sub> H <sub>7</sub> <sup>+</sup> + MCH <sub>4</sub>	100	100	100	NR	29 70 1	NR	100	NR
<i>c</i> -C <sub>3</sub> H <sub>6</sub>	MC <sub>2</sub> H <sub>5</sub> <sup>+</sup> + C <sub>2</sub> H <sub>4</sub> MC <sub>3</sub> H <sub>5</sub> <sup>+</sup> + HL MC <sub>4</sub> H <sub>7</sub> <sup>+</sup> + H <sub>2</sub>	× ×	× ×	× ×	100	87 4 7	100	100	100
<i>n</i> -C <sub>4</sub> H <sub>10</sub>	MC <sub>4</sub> H <sub>9</sub> <sup>+</sup> + HL MC <sub>4</sub> H <sub>7</sub> <sup>+</sup> + HL + H <sub>2</sub> MC <sub>3</sub> H <sub>5</sub> <sup>+</sup> + HL + CH <sub>4</sub> MC <sub>2</sub> H <sub>4</sub> L <sup>+</sup> + C <sub>2</sub> H <sub>6</sub> MC <sub>4</sub> H <sub>8</sub> L <sup>+</sup> + H <sub>2</sub>	40 60	100	23 77	NR	100	NR	48 5 18 29	NR
<i>n</i> -C <sub>5</sub> H <sub>12</sub>	MC <sub>5</sub> H <sub>12</sub> L <sup>+</sup> MC <sub>5</sub> H <sub>10</sub> L <sup>+</sup> + H <sub>2</sub> MC <sub>5</sub> H <sub>8</sub> L <sup>+</sup> + 2H <sub>2</sub> MC <sub>5</sub> H <sub>7</sub> <sup>+</sup> + HL + H <sub>2</sub> MC <sub>4</sub> H <sub>7</sub> <sup>+</sup> + 2CH <sub>4</sub> MC <sub>3</sub> H <sub>6</sub> L <sup>+</sup> + C <sub>2</sub> H <sub>6</sub> MC <sub>3</sub> H <sub>5</sub> <sup>+</sup> + HL + C <sub>2</sub> H <sub>6</sub> MC <sub>2</sub> H <sub>4</sub> L <sup>+</sup> + C <sub>3</sub> H <sub>8</sub> C <sub>5</sub> H <sub>11</sub> <sup>+</sup> + CoCH <sub>4</sub>	× ×	× ×	× ×	NR	NR	NR	30 9 5 51 20 11 4	70

× × indicates the reaction was not performed.




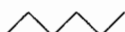
similar reactivity to that observed for  $\text{FeO}^+$ , but the C—C cleavage pathway involving radical loss products is almost completely suppressed. The overall reactivity of  $\text{MS}^+$  is somewhat lower than that for  $\text{FeO}^+$ , with less extensive dehydrogenation observed. This was accounted for as being due to the lower exothermicity of  $\text{H}_2\text{S}$  loss relative to  $\text{H}_2\text{O}$  loss.

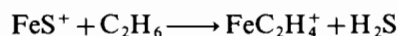
$$\text{Fe}^+ + \text{C}_2\text{H}_6 \longrightarrow \text{FeC}_2\text{H}_4^+ + \text{H}_2$$
$$\Delta H(\text{reaction}) \text{ kcal mol}^{-1} \sim 0 \quad (39)$$


**Scheme 3.**

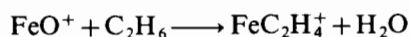


Table 6. Product distributions for the reaction of  $\text{Fe}^+$  and  $\text{FeO}^+$  with linear alkanes

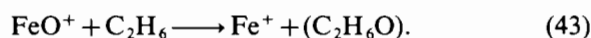
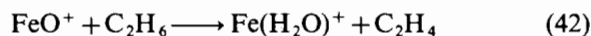
Alkane	$\text{Fe}^+$		$\text{FeO}^+$	
	Neutral lost	% of total	Neutral lost	% of total
$\text{CH}_4$	NR		NR	
$\text{C}_2\text{H}_6$	NR		$\text{H}_2\text{O}$	70
			$\text{C}_2\text{H}_4$	20
			$\text{H}_2\text{O} + \text{C}_2\text{H}_4$	10
	$\text{CH}_4$	76	$\text{H}_2\text{O}$	50
	$\text{H}_2$	24	$\text{CH}_3$	20
			$\text{H}_2\text{O} + \text{C}_3\text{H}_6$	20
			$\text{C}_3\text{H}_6$	10
	$\text{C}_2\text{H}_6$	60	$\text{H}_2\text{O}, \text{H}_2$	60
	$\text{CH}_4$	29	$\text{H}_2\text{O}, \text{C}_2\text{H}_4$	30
	$2\text{H}_2$	3		
	$\text{H}_2$	8	$\text{H}_2\text{O}, \text{C}_4\text{H}_8$	10
	$\text{C}_3\text{H}_8$	43	$\text{H}_2\text{O}, \text{C}_2\text{H}_4$	44
	$\text{CH}_4$	22	$\text{H}_2\text{O}, \text{C}_3\text{H}_6$	27
	$\text{H}_2$	16	$\text{H}_2\text{O}, \text{CH}_4$	15
	$\text{C}_2\text{H}_6$	15	$\text{CH}_3\text{CH}_2$	9
	$\text{C}_2\text{H}_4, \text{H}_2$	4	$\text{H}_2\text{O}, \text{C}_5\text{H}_{10}$	5
	$\text{C}_4\text{H}_{10}$	31	$\text{H}_2\text{O}, \text{C}_3\text{H}_6$	34
	$\text{H}_2$	27	$\text{H}_2\text{O}, \text{C}_2\text{H}_4$	21
	$\text{CH}_4$	13	$\text{H}_2\text{O}, 3\text{H}_2$	15
	$\text{C}_3\text{H}_8$	11	$\text{CH}_3\text{CH}_2$	14
	$\text{C}_2\text{H}_6$	11	$\text{H}_2\text{O}, \text{C}_2\text{H}_4, \text{H}_2$	9
	$\text{C}_2\text{H}_6, \text{H}_2$	7	$\text{H}_2\text{O}, \text{C}_4\text{H}_8$	7



$$\Delta H(\text{reaction}) \text{ kcal mol}^{-1} \sim -8 \quad (40)$$



$$\Delta H(\text{reaction}) \text{ kcal mol}^{-1} \sim -51 \quad (41)$$



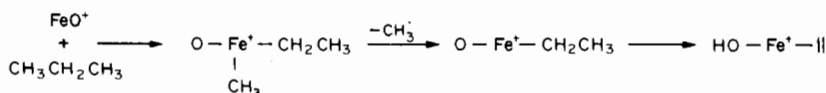
Reactions (39)–(41) show the overall exothermicity of reaction of  $\text{FeL}^+$  ( $\text{L} = \text{O}, \text{S}$ ) and  $\text{Fe}^+$  with ethane.

$\text{L} = \text{CH}_2, \text{NH}$ . Transition metal carbenes are very important in organometallic chemistry due to their presence as intermediates in many important

catalytic processes. Because of this and the fact that they can be easily generated, there have been numerous studies on their chemistry and photochemistry.

Table 7 shows product distributions for the reactions of  $\text{RhCH}_2^+$ ,  $\text{FeCH}_2^+$  and  $\text{CoCH}_2^+$  with a few alkanes and alkenes. These carbenes exhibit very complex chemistry including migratory insertion, olefin metathesis, olefin homologation and other pathways.<sup>18(c)-(e),49</sup>

Scheme 5 shows proposed reaction pathways for  $\text{CoCH}_2^+$  with ethane. Numerous steps show migratory insertion of  $\text{CH}_2$  into an  $\text{M}-\text{C}$  bond. Analogous behaviour is seen with  $\text{RhCH}_2^+$  and  $\text{FeCH}_2^+$  with alkanes and also with  $\text{MCH}_2^+$



Scheme 4.

Table 7. Product distributions for reactions of  $MCH_2^+$  with various hydrocarbons ( $M = Fe, Co, Rh$ )

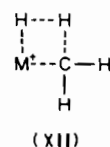
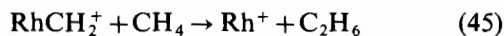
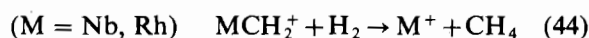
Reactant	Product	$FeCH_2^+$	$CoCH_2^+$	$RhCH_2^+$
$C_2H_4$	$M^+ + C_3H_6$	100	100	30
	$MC_3H_4^+ + H_2$			70
$C_3H_6$	$M^+ + C_4H_8$	32	31	8
	$MC_2H_4^+ + C_2H_4$	62	54	27
	$MC_3H_4^+ + CH_4$			26
	$MC_4H_4^+ + 2H_2$			23
	$MC_4H_6^+ + H_2$	6	15	16
$C_2H_6$	$M^+ + C_3H_8$	NR	58	8
	$MC_2H_4^+ + CH_4$		28	92
	$MC_3H_6^+ + H_2$		14	
$C_3H_8$	$M^+ + C_4H_{10}$	16	18	$\times \times$
	$MC_2H_4^+ + C_2H_6$	8	13	
	$MC_3H_6^+ + CH_4$	70	59	
	$MC_4H_6^+ + 2H_2$	2	1	
	$MC_4H_8^+ + H_2$	4	9	

NR indicates no reaction was observed ( $k^{II} < 10^{-12} \text{ cm}^3 \text{ mol}^{-1} \text{ s}^{-1}$ ).

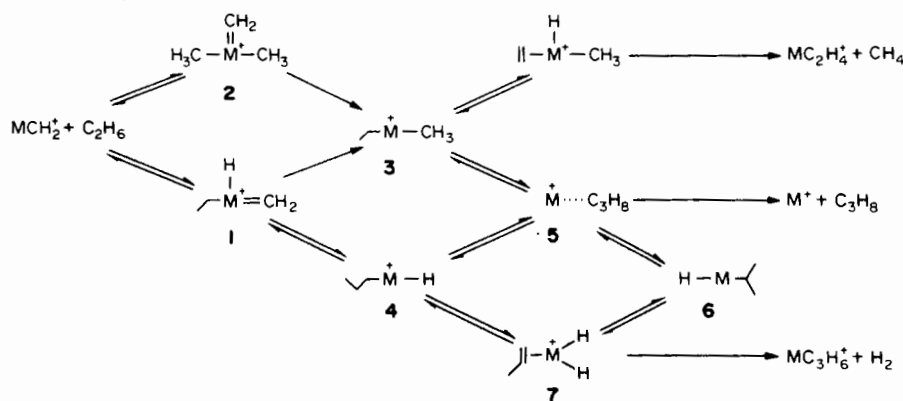
$\times \times$  indicates the reaction was not performed.

( $M = Fe, Co$ ) with alkenes.<sup>18(f)</sup> It was proposed that the positive charge on the metal centre makes the unsaturated carbon electrophilic. The alkyl group then migrates with its bonding pair onto the unsaturated carbon.

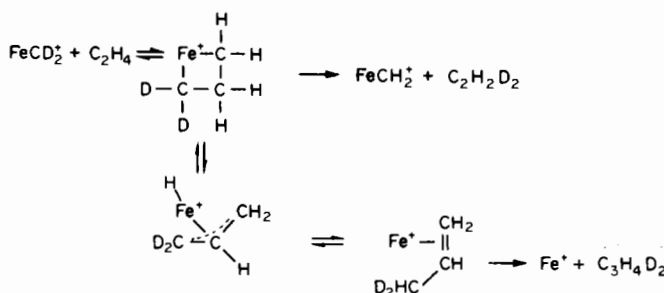
$RhCH_2^+$  and  $NbCH_2^+$  are observed to react with both  $H_2$  and  $CH_4$ , reactions (44)–(46).<sup>49,50</sup> Reaction (44) is proposed to have a four-centred intermediate like structure (XII).



Four-centred intermediates are also proposed for the reactions of  $MCH_2^+$  ( $M = Fe, Co$ ) and  $FeNH^+$  with alkenes.<sup>16,18</sup> For example,  $FeCD_2^+$  reacts with ethene (for products see Table 7) as in reactions (47) and (48). A mechanism which accounts for this is shown in Scheme 6, with a four-centred intermediate. Metallocyclic intermediates of this type

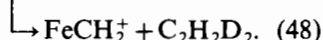
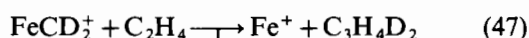


Scheme 5.

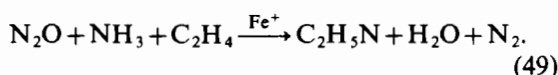


Scheme 6.

have also been observed in condensed phase.



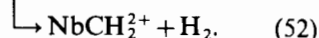
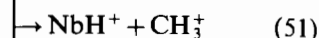
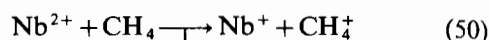
$\text{FeNH}^+$  reacts with ethene via several reaction pathways including a metathesis reaction to form  $\text{FeCH}_2^+$  and a homologation reaction to produce  $\text{Fe}^+$ .<sup>16</sup> These products indicate  $\text{Fe}^+$  catalysed formation of an N—C bond, reaction (49), which is one of the first of its kind.



A mechanism consistent with these results is shown in Scheme 7.

The reaction of  $\text{FeO}^+$  with  $\text{C}_2\text{H}_4$  generates products analogous to those in the  $\text{FeNH}^+/\text{C}_2\text{H}_4$  reaction. This suggests a generalized mechanism for reaction of the isoelectronic series  $\text{FeNH}^+$ ,  $\text{FeCH}_2^+$ ,  $\text{FeO}^+$  with  $\text{C}_2\text{H}_4$ , Scheme 8.

Multiply charged metal ions have been observed to react almost exclusively via rapid charge exchange. Recently, however, we reported that  $\text{Nb}^{2+}$  reacts with  $\text{CH}_4$  as in reactions (50)–(52).<sup>51</sup>  $\text{NbCH}_2^{2+}$  formed in reaction (52) is observed to undergo rapid proton transfer to form  $\text{NbCH}^+$ . These studies yielded  $D^0(\text{Nb}^{2+}-\text{CH}_2) = 197 \pm 10$  kcal mol<sup>-1</sup> in comparison to  $D^0(\text{Nb}^+-\text{CH}_2) = 109 \pm 5$  kcal mol<sup>-1</sup>.



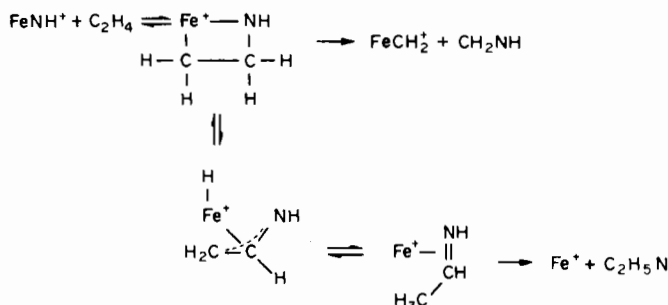
The effect of a multiple charge on the bond energies and reactivities of metal–ligand species will be the subject of further investigation.

$L = \pi$ -type ligands. A number of novel reactions have been observed in the reactions of metal–olefin ion complexes. All of the reactions with hydrocarbons so far have involved some neutral losses (dehydrogenation, dealkylation, dehydration, loss of a ligand, etc.) to eliminate excess energy and stabilize the newly formed complex. However,  $\text{RhC}_7\text{H}_6^+$ , formed in reaction (53), reacts with  $\text{H}_2$  to undergo the hydrogenation reaction (54).<sup>52</sup>

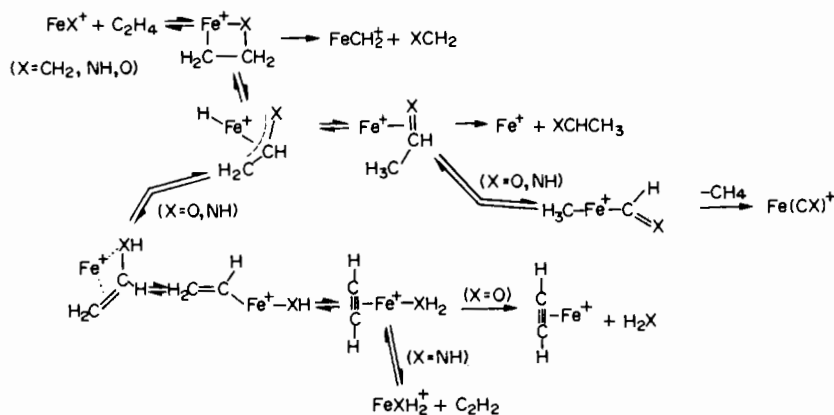


This reaction is observed to go to completion with a rate constant of  $(6 \pm 3) \times 10^{-11}$  cm<sup>3</sup> molecule<sup>-1</sup> s<sup>-1</sup>. The product ion,  $\text{RhC}_7\text{H}_8^+$ , was proposed to be stabilized by IR radiative stabilization.

$\text{Co}(\text{Cp})^+$  reacts with alkanes by similar pathways to  $\text{Co}(\text{allyl})^+$ .<sup>53</sup> As previously discussed,  $\text{Co}(\text{allyl})^+$  reacts mainly via dehydrogenation without coupling of the ligands. In a novel reaction,  $\text{Co}(\text{Cp})(\text{alkene})^+$  complexes for  $\text{C}_5$  and  $\text{C}_6$  alkenes undergo collisionally activated dehydrocyclization to form  $\text{Co}(\text{Cp})_2^+$ . As expected, this reaction occurs more readily for linear alkenes than for branched alkenes.  $\text{Co}(\text{Cp})^+$  also reacts with trans-1,3-pentadiene to

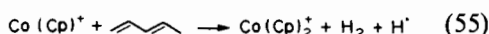


Scheme 7.

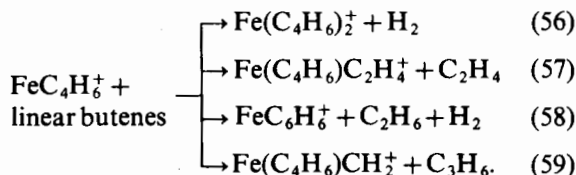


Scheme 8.

form  $\text{Co}(\text{Cp})_2^+$ , reaction (55).



Studies of  $\text{M}(\text{alkene})^+$  show that enhancement or reduction of available reaction routes can occur upon attachment of an alkene.<sup>16,45,54</sup> For  $\text{Fe}^+$ , reaction with 1-butene produces  $\text{Fe}(\text{butadiene})^+$ , exclusively.<sup>45</sup>  $\text{Fe}(\text{butadiene})^+$  reacts with linear butenes via numerous reaction routes, reactions (56)–(59).



In contrast,  $\text{Sc}^+$ ,  $\text{Y}^+$  and  $\text{La}^+$  react more slowly and with fewer reaction pathways in their secondary reactions with alkanes relative to their primary reactions.<sup>16,54</sup> For example,  $\text{La}(\text{alkene})^+$  only reacts with  $\text{C}_3$ – $\text{C}_5$  cyclic alkenes, whereas  $\text{La}^+$  reacts with  $\text{C}_2$  and larger linear, cyclic and branched alkanes.

## CONCLUSION

FTMS has been proven to be an excellent technique for generating and studying highly unsaturated metal-ligand ions. Many novel species including bare metal carbenes, alkyls, hydrides, amides, nitrenes, etc. can be prepared. Subsequent ion-molecule reactions and photodissociation have been used to derive thermodynamic information which is useful for proposing mechanisms and structures. The development of these tools will allow a fuller understanding of the effect of ligands on gas-phase metal ion reactivity.

Future directions for this research will be to investigate the effect of a second ligand on the bond strength of the first ligand as well as its effect on the

overall reactivity. We have also recently observed marked changes in the reactivity of small transition metal cluster ions upon the addition of a ligand.<sup>55</sup> Clearly, the surface has just been scratched!

**Acknowledgements**—Metal-ligand ion research in our laboratory is supported by the Division of Chemical Sciences in the Office of Basic Energy Research in the United States Department of Energy (DE-FG02-87ER13766) and the National Science Foundation (CHE-8612234). S.W.B. also acknowledges the W. R. Grace Company for providing fellowship support.

## REFERENCES

1. J. Allison, R. B. Freas and D. P. Ridge, *J. Am. Chem. Soc.* 1979, **101**, 1332.
2. For a review of gas phase metal-ion chemistry, see: J. Allison, in *Progress in Inorganic Chemistry*, Vol. 34, p. 628. (Edited by S. J. Lippard.) Wiley-Interscience, New York (1986).
3. (a) J. Allison and D. P. Ridge, *J. Am. Chem. Soc.* 1979, **101**, 4998; (b) A. Tsarbopoulos and J. Allison, *Organometallics* 1984, **3**, 86; (c) R. C. Burnier, G. D. Byrd and B. S. Freiser, *J. Am. Chem. Soc.* 1981, **103**, 4360; (d) D. B. Jacobson and B. S. Freiser, *J. Am. Chem. Soc.* 1983, **105**, 5797; (e) R. Houriet, L. F. Halle and J. L. Beauchamp, *Organometallics* 1983, **2**, 1818; (f) J. L. Elkind and P. B. Armentrout, *J. Am. Chem. Soc.* 1986, **108**, 2765; (g) D. A. Weil and C. L. Wilkins, *J. Am. Chem. Soc.* 1986, **108**, 2765; (h) D. A. Peake and M. L. Gross, *J. Am. Chem. Soc.* 1987, **109**, 600; (i) C. Schulze, H. Schwarz, D. A. Peake and M. L. Gross, *J. Am. Chem. Soc.* 1987, **109**, 2368.
4. (a) J. L. Elkind and P. B. Armentrout, *J. Chem. Phys.* 1986, **84**, 1986; (b) P. B. Armentrout, J. L. Beauchamp and R. V. Hodges, *J. Chem. Phys.* 1977, **66**, 4683.
5. (a) M. B. Comisarow and A. G. Marshall, *Chem. Phys. Lett.* 1974, **25**, 282; (b) M. B. Comisarow and A. G. Marshall, *Chem. Phys. Lett.* 1974, **26**, 489; (c)

- M. B. Comisarow and A. G. Marshall, *Can. J. Chem.* 1974, **52**, 1997.
6. (a) B. S. Freiser, *Talanta* 1985, **32**, 697; (b) T. J. Carlin, M. B. Wise and B. S. Freiser, *Inorg. Chem.* 1981, **20**, 2743.
7. (a) R. Tonkyn and J. C. Weisshaar, *J. Phys. Chem.* 1986, **90**, 2305; (b) D. Wang and R. R. Squires, *Organometallics* 1985, **6**, 697.
8. R. B. Cody, R. C. Burnier, W. D. Reents Jr, T. J. Carlin, D. A. McCrery, R. K. Lengal and B. S. Freiser, *Int. J. Mass Spec. Ion Phys.* 1980, **33**, 37.
9. (a) R. Georgiadis and P. B. Armentrout, *J. Am. Chem. Soc.* 1986, **108**, 2119; (b) P. B. Armentrout and J. L. Beauchamp, *Chem. Phys.* 1980, **48**, 315.
10. (a) D. A. Peake, M. L. Gross and D. P. Ridge, *J. Am. Chem. Soc.* 1984, **106**, 4307; (b) R. B. Cody and B. S. Freiser, *Int. J. Mass Spec. Ion Phys.* 1982, **41**, 199; (c) R. G. Cooks, *Collision Spectroscopy*. Plenum, New York (1978).
11. R. C. Dunbar, *Gas Phase Ion Chemistry*, Vol. 3, Chap. 20. (Edited by M. T. Bowers.) Academic Press, New York (1984).
12. (a) D. A. Laude, C. L. Johlman, R. S. Brown, D. A. Weil and C. L. Wilkins, *Mass Spec. Rev.* 1986, **5**, 107 and refs cited within; (b) A. G. Marshall, *Acc. Chem. Res.* 1985, **18**, 316.
13. M. B. Comisarow, G. Parisod and V. Grassi, *Chem. Phys. Lett.* 1978, **57**, 413.
14. (a) M. Bensimon and R. Houriet, *Int. J. Mass Spec. Ion. Proc.* 1986, **72**, 93; (b) R. A. Forbes, L. M. Lech and B. S. Freiser, *Int. J. Mass Spec. Ion. Proc.* 1987, **77**, 107.
15. H. Kang and J. L. Beauchamp, *J. Phys. Chem.* 1985, **89**, 3364.
16. L. M. Lech, S. W. Buckner, Y. Huang, T. J. MacMahon, J. R. Gord and B. S. Freiser, unpublished results.
17. T. J. Carlin and B. S. Freiser, *Anal. Chem.* 1983, **55**, 571.
18. (a) D. B. Jacobson and B. S. Freiser, *J. Am. Chem. Soc.* 1984, **106**, 3891; (b) D. B. Jacobson and B. S. Freiser, *J. Am. Chem. Soc.* 1984, **106**, 3900; (c) D. B. Jacobson and B. S. Freiser, *J. Am. Chem. Soc.* 1985, **107**, 67; (d) D. B. Jacobson and B. S. Freiser, *J. Am. Chem. Soc.* 1985, **107**, 2605; (e) D. B. Jacobson and B. S. Freiser, *J. Am. Chem. Soc.* 1985, **107**, 4373; (f) D. B. Jacobson and B. S. Freiser, *J. Am. Chem. Soc.* 1985, **107**, 5876.
19. (a) T. J. Carlin, L. Sallans, C. J. Cassidy, D. B. Jacobson and B. S. Freiser, *J. Am. Chem. Soc.* 1983, **105**, 6320; (b) D. B. Jacobson and B. S. Freiser, *J. Am. Chem. Soc.* 1984, **106**, 4623; (c) D. B. Jacobson and B. S. Freiser, *J. Am. Chem. Soc.* 1984, **106**, 5351.
20. R. L. Hettich, T. C. Jackson, E. M. Stanko and B. S. Freiser, *J. Am. Chem. Soc.* 1986, **108**, 5086.
21. R. L. Hettich and B. S. Freiser, *J. Am. Chem. Soc.* 1986, **108**, 2537.
22. D. B. Jacobson and B. S. Freiser, *J. Am. Chem. Soc.* 1983, **105**, 736.
23. P. B. Armentrout, L. F. Halle and J. L. Beauchamp, *J. Am. Chem. Soc.* 1981, **103**, 6624.
24. (a) G. D. Byrd and B. S. Freiser, *J. Am. Chem. Soc.* 1982, **104**, 5944; (b) D. B. Jacobson and B. S. Freiser, *J. Am. Chem. Soc.* 1985, **107**, 72.
25. D. B. Jacobson and B. S. Freiser, *Organometallics* 1984, **3**, 513.
26. S. W. Buckner and B. S. Freiser, *J. Am. Chem. Soc.* 1987, **109**, 4715.
27. L. F. Halle, R. Houriet, M. Kappes, R. H. Staley and J. L. Beauchamp, *J. Am. Chem. Soc.* 1982, **104**, 6293.
28. E. Murad, *J. Chem. Phys.* 1980, **73**, 1381.
29. R. R. Corderman and J. L. Beauchamp, *J. Am. Chem. Soc.* 1976, **98**, 3998.
30. (a) R. W. Jones and R. H. Staley, *Int. J. Mass Spec. Ion. Phys.* 1981, **39**, 35; (b) J. S. Uppal and R. H. Staley, *J. Am. Chem. Soc.* 1982, **104**, 1235.
31. C. J. Cassidy and B. S. Freiser, *J. Am. Chem. Soc.* 1984, **106**, 6176.
32. (a) R. G. Cooks and T. L. Kruger, *J. Am. Chem. Soc.* 1977, **99**, 1279; (b) S. A. McLuckey, D. Cameron and R. G. Cooks, *J. Am. Chem. Soc.* 1981, **103**, 1313; (c) S. A. McLuckey, A. E. Schoen and R. G. Cooks, *J. Am. Chem. Soc.* 1982, **104**, 848.
33. P. B. Armentrout and J. L. Beauchamp, *J. Am. Chem. Soc.* 1981, **103**, 784.
34. J. L. Beauchamp, private communication.
35. M. Mautner, *J. Am. Chem. Soc.* 1982, **104**, 5.
36. L. Sallans, K. R. Lane, R. R. Squires and B. S. Freiser, *J. Am. Chem. Soc.* 1985, **107**, 4379.
37. L. Operti, E. C. Tews and B. S. Freiser, *J. Am. Chem. Soc.*, in press.
38. P. B. Armentrout, private communication.
39. P. B. Armentrout and J. L. Beauchamp, *J. Am. Chem. Soc.* 1981, **103**, 784.
40. M. F. Lappert, P. P. Power, A. R. Sanger and R. C. Srivastava, *Metal and Metalloid Amides*. Ellis Horwood Ltd, West Sussex, U.K. (1980).
41. (a) J. Allison and B. D. Radecki, *J. Am. Chem. Soc.* 1984, **106**, 946; (b) S. J. Babinec and J. Allison, *J. Am. Chem. Soc.* 1984, **106**, 7718.
42. H. E. Bryndza, L. K. Fong, R. A. Paciello, W. Tam and J. E. Bercaw, *J. Am. Chem. Soc.* 1987, **109**, 1444.
43. N. Aristov and P. B. Armentrout, *J. Am. Chem. Soc.* 1984, **106**, 4065.
44. C. J. Cassidy and B. S. Freiser, *J. Am. Chem. Soc.* 1986, **108**, 5690.
45. D. B. Jacobson and B. S. Freiser, *J. Am. Chem. Soc.* 1983, **105**, 7484.
46. T. C. Jackson, D. B. Jacobson and B. S. Freiser, *J. Am. Chem. Soc.* 1984, **106**, 1252.
47. T. C. Jackson, T. J. Carlin and B. S. Freiser, *J. Am. Chem. Soc.* 1986, **108**, 1120.
48. T. C. Jackson, T. J. Carlin and B. S. Freiser, *Int. J. Mass Spec. Ion. Proc.* 1986, **72**, 169.
49. D. B. Jacobson and B. S. Freiser, *J. Am. Chem. Soc.* 1985, **107**, 5870.
50. R. L. Hettich and B. S. Freiser, *J. Am. Chem. Soc.* 1987, **109**, 3543.
51. S. W. Buckner and B. S. Freiser, *J. Am. Chem. Soc.* 1987, **109**, 1247.

52. D. B. Jacobson and B. S. Freiser, *J. Am. Chem. Soc.* 1984, **106**, 1159.
53. D. B. Jacobson and B. S. Freiser, *J. Am. Chem. Soc.* 1985, **107**, 7399.
54. Y. Huang, M. B. Wise, D. B. Jacobson and B. S. Freiser, *Organometallics* 1987, **6**, 346.
55. S. W. Buckner, J. R. Gord and B. S. Freiser, *J. Chem. Phys.* 1988, **88**, 3678.
56. R. C. Burnier and B. S. Freiser, *Inorg. Chem.* 1979, **18**, 906.
57. P. B. Armentrout and J. L. Beauchamp, *J. Chem. Phys.* 1981, **74**, 2819.
58. P. B. Armentrout, L. F. Halle and J. L. Beauchamp, *J. Am. Chem. Soc.* 1981, **103**, 6501.
59. D. B. Jacobson, G. D. Byrd and B. S. Freiser, *Inorg. Chem.* 1984, **23**, 553.
60. L. F. Halle, P. B. Armentrout and J. L. Beauchamp, *Organometallics* 1982, **1**, 963.
61. S. Evans, M. F. Guest, I. H. Hillier and E. F. Orchard, *J. Chem. Soc., Faraday Trans. II* 1974, **70**, 417.
62. J. L. Elkind and P. B. Armentrout, *Inorg. Chem.* 1986, **25**, 1078.
63. D. B. Jacobson, private communication.